Reactance Compensation Control for Multiple-Receiver Wireless Power Transfer System with Coil Inductance Variations

Ryo Matsumoto*, Hiroshi Fujimoto†
*Graduate School of Frontier Sciences, The University of Tokyo, Kashiwa, Japan
*matsumoto.ryo19@ae.k.u-tokyo.ac.jp, †fujimoto@k.u-tokyo.ac.jp

***Abstract*—In practical multiple-receiver wireless power transfer systems, the parameters of the coils and capacitors may vary from their designed values, thus preventing the reactance of the transmitter and receiver coils from being completely compensated. This paper proposes a control scheme for pulsewidth modulation controlled switched capacitors to compensate for the self-inductance variations of the coils and maintain the transmission efficiency. The proposed control scheme is implemented by completely separate closed-loops on each circuit to avoid wireless communication, which has been a major challenge in previous methods. The effectiveness of the proposed control scheme is verified by an experimental prototype consisting of a single transmitter coil and two receiver coils.**

***Index Terms*—Multiple receiver, switched capacitor, wireless power transfer (WPT).**

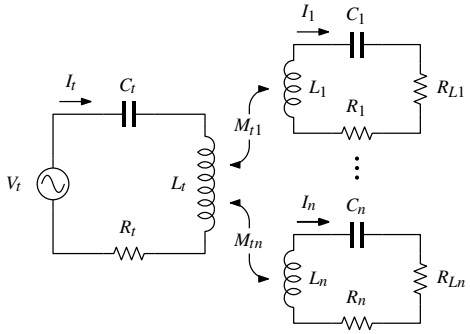

Fig. 1. Simplified circuit of a multiple-receiver WPT system.

I. Introduction

Wireless power transfer (WPT) via magnetic resonance coupling is attracting attention from the industry for its convenience and safety. One advantage of this technology is the ability to transfer power to multiple receivers from a single transmitter coil [1]–[15]. Applications of multiple-receiver WPT include mobile devices, household appliances, sensors, and so on.

Typical WPT systems adopt compensation capacitors on the transmitter (TX) and receiver (RX) circuits to compensate for the reactance of the TX and RX coils [16]. However, in practical applications, the parameters of the coils and capacitors may vary from their designed values, thus preventing the reactance from being completely compensated. Several methods have been proposed in the literature to address this issue. In [17], [18], variable capacitors or active rectifiers have been adopted to compensate for the unnecessary reactance in single-receiver WPT systems. In [19], [20], variable capacitors have been adopted in multiple-receiver WPT systems to compensate for the parameter variations and cross interference among individual receivers. The control scheme of the variable capacitors in [19], [20] use the phase difference between the TX current and RX current as the feedback information. Wireless communication [19] or additional circuits [20] are required to obtain the phase difference, which remains to be a major limitation from a practical point of view.

This paper addresses the issue of parameter variations in multiple-receiver WPT systems and proposes a practical control scheme for pulsewidth modulation (PWM) controlled switched capacitors. The control scheme proposed in this paper can be implemented by completely separate closed-loops on each circuit, thus eliminating wireless communication and additional circuits. The basis of the proposed control scheme is the constant amplitude control of the TX current, which is necessary to mitigate the interference between individual receivers [19], [20].

II. Proposed Control Scheme

In multiple-receiver WPT systems, the power transferred to one receiver can be affected by the position and load condition of other receivers. A detailed description of this phenomenon and a solution to isolate the power flow to each receiver is provided in Section II-A. Based on the discussion in Section II-A, a control scheme for PWM-controlled switched capacitors is proposed in Section II-B to adapt to self-inductance variations and improve the transmission efficiency.

A. Independent Power Transfer to Multiple Receivers

Fig. 1 shows a simplified circuit of a multiple-receiver WPT system. V_t represents the AC voltage applied to the TX circuit. L_t, C_t, and R_t represent the self-inductance of the TX coil, the compensation capacitance of the TX circuit, and the equivalent series resistance (ESR) of the TX circuit, respectively. L_k, C_k, R_k, and R_{Lk} $(k = 1, ..., n)$ represent the self-inductance of the k-th RX coil, the compensation capacitance of the k-th RX circuit, the ESR of the k-th RX circuit, and the load resistance of the k-th RX circuit, respectively. M_{tk} $(k = 1, ..., n)$ represents the mutual inductance between the TX coil and

the k-th RX coil. In this paper, the distance between the receivers are assumed to be sufficiently large such that the mutual inductance between the RX coils can be neglected. The reactance of the TX circuit and the k-th RX circuit are defined as:

$$jX_t := j\omega L_t + \frac{1}{j\omega C_t}, \tag{1}$$

$$jX_k := j\omega L_k + \frac{1}{j\omega C_k} \quad (k = 1, ..., n). \tag{2}$$

When the reactance of the TX and RX coils are perfectly compensated, X_t and X_k are equal to zero. However, when the self-inductance of the coils vary from their designed values, X_t and X_k are not equal to zero. The effects of X_t and X_k on the power transfer characteristics will be discussed in detail in Section II-B.

By applying Kirchhoff's voltage law to the circuit in Fig. 1, the following equations can be obtained:

$$V_t = (jX_t + R_t)I_t - \sum_{k=1}^{n}(j\omega M_{tk})I_k, \tag{3}$$

$$j\omega M_{tk} I_t = (jX_k + R_k + R_{Lk})I_k \quad (k = 1, ..., n). \tag{4}$$

By solving (3) and (4), I_t can be expressed in terms of V_t as:

$$I_t = \frac{V_t}{jX_t + R_t + \sum_{k=1}^{n} \frac{(\omega M_{tk})^2}{jX_k + R_k + R_{Lk}}}. \tag{5}$$

The power delivered to the load of the k-th RX circuit can be expressed in terms of I_t as:

$$P_{Lk} = R_{Lk}|I_k|^2 = \frac{R_{Lk}(\omega M_{tk})^2 |I_t|^2}{X_k^2 + (R_k + R_{Lk})^2} \quad (k = 1, ..., n). \tag{6}$$

It can be seen from (5) and (6) that when V_t is constant, P_{Lk} is affected by the mutual inductance between the TX coil and all RX coils, and also the load resistance of all RX circuits. In fact, the power transferred to one receiver is affected by the position and load condition of other receivers. Obviously, the output power of each receiver becomes unstable under such conditions.

It can also be seen from (6) that when the amplitude of I_t is constant, P_{Lk} is solely determined by the mutual inductance between the TX coil and the k-th RX coil, and the load resistance of the k-th RX circuit. This condition is favorable in terms of stability since the power transferred to one receiver is unaffected by the existence of other receivers. The amplitude of I_t can be kept constant by adopting the LCC topology [21] on the TX circuit or by applying feedback control and modulating the pulse-width of the inverter. The latter method is adopted in this paper since the volume and cost of the system can be reduced compared to the former method.

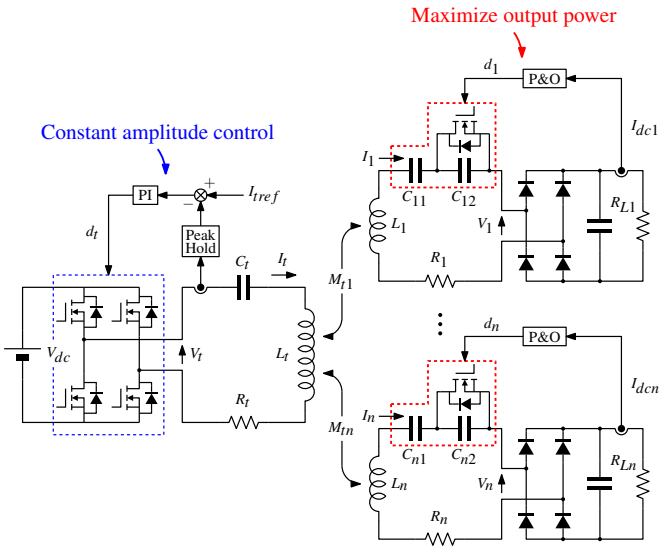

Fig. 2. Overview of the proposed control scheme.

B. Reactance Compensation Using PWM-Controlled Switched Capacitors

The Joule losses caused by the ESR of the TX circuit and the ESR of the k-th RX circuit can be expressed as:

$$P_t = R_t|I_t|^2, \qquad P_k = R_k|I_k|^2 \quad (k = 1, ..., n). \tag{7}$$

Assuming that the amplitude of I_t is constant, the transmission efficiency to the k-th receiver can be expressed as:

$$\eta_k = \frac{P_{Lk}}{P_t + \sum_{i=1}^{n} P_i + \sum_{i=1}^{n} P_{Li}} = \frac{\frac{R_{Lk}(\omega M_{tk})^2}{X_k^2 + (R_k + R_{Lk})^2}}{R_t + \sum_{i=1}^{n} \frac{(R_i + R_{Li})(\omega M_{ti})^2}{X_i^2 + (R_i + R_{Li})^2}}. \tag{8}$$

It can be seen from (8) that the maximum η_k in terms of X_k is obtained under $X_k = 0$. In other words, the transmission efficiency to the k-th receiver is maximized when the reactance of the k-th circuit is completely compensated. Therefore, the transmission efficiency to each receiver is maximized under $X_1 = ... = X_n = 0$. It can also be seen from (8) that the transmission efficiency does not depend on X_t. These analyses indicate that the transmission efficiency can be maintained by adopting variable capacitors on each RX circuit and compensating for the self-inductance variations of the RX coils.

Fig. 2 shows the overview of the proposed control scheme. The amplitude of the TX current is regulated to a constant value by a PI controller. PWM-controlled switched capacitors [22]–[24] are adopted in each RX circuit instead of passive compensation capacitors. The equivalent capacitance of the switched capacitor of the k-th receiver is given by:

$$C_k = \frac{1}{\frac{1}{C_{k1}} + \frac{1}{C_{k2}}\left[1 + \frac{1}{2\pi}\sin(2\pi d_k) - d_k\right]} \tag{9}$$

where d_k is the duty cycle of the PWM signal applied to the MOSFET [23]. The most basic approach to determine

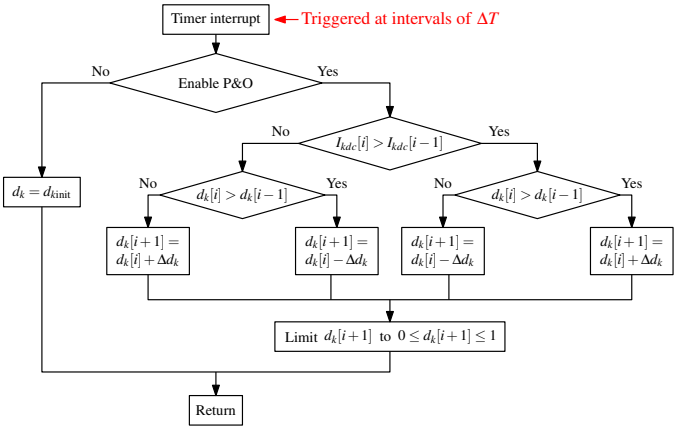

Fig. 3. Flowchart of the P&O algorithm.

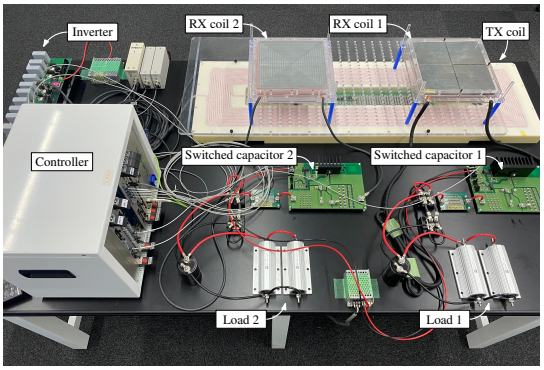

Fig. 4. Experimental setup.

TABLE I
SPECIFICATIONS OF EXPERIMENTAL SETUP.

Description	Symbol	Value
Operating frequency	-	85.0 kHz
Input DC voltage	V_{dc}	50.0 V
Reference of TX current amplitude	I_{tref}	5.0 A
Self-inductance of TX	L_t	259.0 µH
Self-inductance of RX1	L_1	101.2 µH
Self-inductance of RX2	L_2	99.7 µH
Load resistance of receiver 1	R_{L1}	11.0 Ω
Load resistance of receiver 2	R_{L2}	11.0 Ω
ESR of transmitter	R_t	194.2 mΩ
ESR of receiver 1	R_1	76.7 mΩ
ESR of receiver 2	R_2	68.7 mΩ
Mutual inductance of TX and RX1	M_{t1}	11.9 µH
Mutual inductance of TX and RX2	M_{t2}	11.7 µH
Mutual inductance of RX1 and RX2	M_{12}	0.5 µH
Series connected capacitors constituting switched capacitor 1	C_{11} C_{12}	43.2 nF 89.2 nF
Series connected capacitors constituting switched capacitor 2	C_{21} C_{22}	44.0 nF 89.4 nF

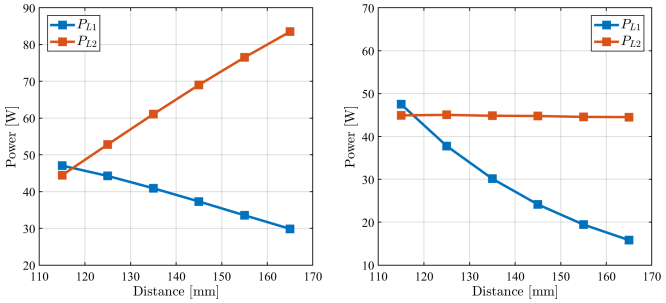

(a) (b)

Fig. 5. Output DC power of RX1 and RX2 according to the vertical airgap between TX coil and RX coil 1. (a) Measurement results when V_t is constant. (b) Measurement results when I_t is regulated to 4 A by the PI controller.

the values of the switched capacitors is to use the information of the current phase. In fact, the reactance of the k-th RX circuit is completely compensated when the phase of I_k leads the phase of I_t by 90° [19], [20]. However, wireless communication between the transmitter and each receiver is required to obtain the phase difference between I_t and I_k. Wireless communication increases the complexity of the system and entails the risk of communication failures. Moreover, this is not a practical solution when considering the latency of wireless communication [25] and the typical operating frequency of WPT systems.

In order to control the switched capacitors without wireless communication, the information of the output power is utilized in the proposed control scheme. It can be seen from (6) that when the amplitude of I_t is constant, the maximum P_{Lk} in terms of X_k is obtained under $X_k = 0$. Therefore, X_k converges to zero by searching the value of d_k which yields the maximum P_{Lk}. In this paper, Perturb & Observe (P&O) algorithms [26] are adopted in each receiver to track the maximum output power. As shown in Fig. 3, d_k is incremented or decremented by a constant step size of Δd_k in each iteration.

As shown in Fig. 2, the proposed control scheme can be implemented by completely separate closed-loops on each circuit, thus eliminating wireless communication and additional circuits. In order to avoid conflict between the PI control and P&O algorithms, the iteration period of the P&O algorithm must be designed sufficiently longer than the settling time of the PI control. The P&O algorithms implemented on each receiver do not conflict with each other when the mutual inductance between the RX coils is negligibly small.

It should be noted that M_{tk} and R_{Lk} can take arbitrary values in the proposed control scheme, as far as M_{tk} and R_{Lk} remain constant during the maximum power tracking process. This indicates the flexibility of the proposed control scheme against variations in coil position and load condition.

III. EXPERIMENTAL VERIFICATION

Fig. 4 shows the experimental setup. The specifications of the setup are listed in Table I. The experiment is conducted using a single transmitter and two receivers to emulate the most basic configuration of multiple-receiver WPT systems. The two receivers are placed such that the mutual inductance between them is sufficiently small. Δd_k is set to 0.005, and ΔT is set to 2 ms. Although not depicted in Fig. 2, a digital low-pass filter (LPF) is applied to reduce the noise of I_{1dc} and I_{2dc}. The cut-off frequency of the LPF is set to 1 kHz.

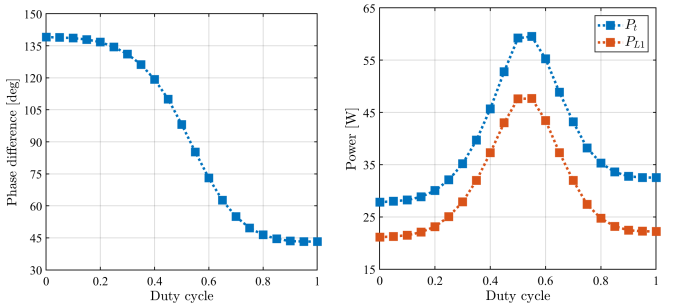

Fig. 6. Steady-state measurements according to the duty cycle of the switched capacitor. (a) Phase difference between I_t and I_1. (b) Input DC power and output DC power of RX1.

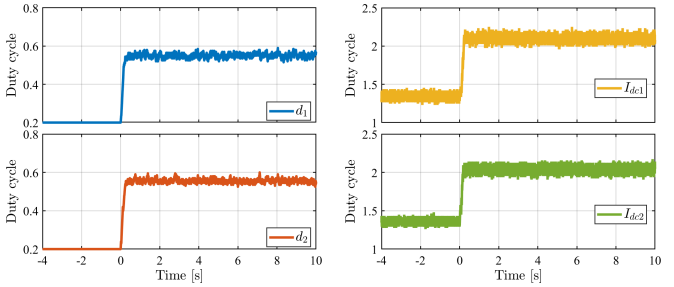

Fig. 7. (a) Trajectories of d_1, d_2 and (b) waveforms of I_{dc1}, I_{dc2} when applying the proposed control scheme under ΔL_1 =0 µH, ΔL_2 =0 µH.

Fig. 5 shows the output DC power of RX1 and RX2 when the vertical airgap between the TX coil and RX coil 1 is varied from 115 mm from 165 mm. The duty cycles of switched capacitors 1 and 2 are both fixed to 0.5. Fig. 5(a) shows that when the constant amplitude control is not applied, the output power of RX2 varies significantly depending on the position of RX1. On the other hand, Fig. 5(b) shows that the output power of RX2 is constant regardless of the position of RX1 when the constant amplitude control is applied. These results validate the discussion in Section II-A.

Fig. 6 shows the measurement results of the phase difference and power when the duty cycle of switched capacitor 1 is incremented in steps of 0.05 from 0 to 1. In this experiment, RX coil 1 is placed in the original position while RX coil 2 is removed from the setup. The amplitude of the TX current is regulated to 5 A. The phase difference between I_t and I_1 is 90° when the duty cycle is between 0.5 and 0.55, indicating that the reactance of RX 1 is compensated by the switched capacitor. In addition, the output power of RX 1 is maximized when the duty cycle is between 0.5 and 0.55. These results indicate that the reactance of RX 1 can be compensated by tracking the maximum output power point, thus verifying the theoretical basis of the control scheme discussed in Section II-B.

Fig. 7(a) shows the trajectories of d_1 and d_2 when the TX current control and P&O algorithms are both applied. d_1 and d_2 settle to a stable value slightly higher than 0.5, which shows

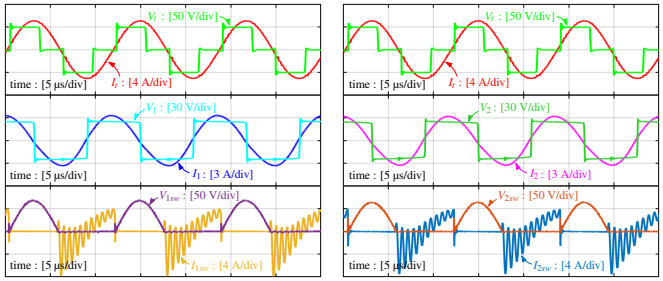

Fig. 8. AC waveforms measured at steady-state when applying the proposed control scheme under ΔL_1 =0 µH, ΔL_2 =0 µH. (a) Waveforms of the transmitter and receiver 1. (b) Waveforms of the transmitter and receiver 2.

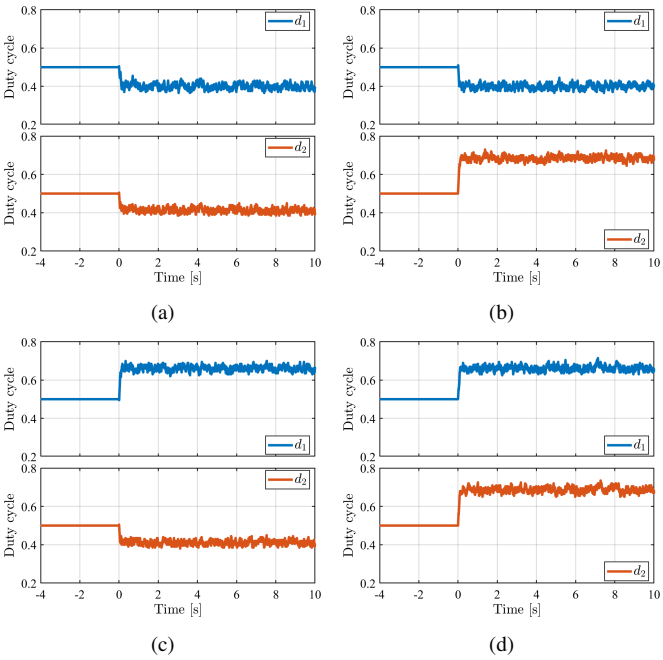

Fig. 9. Trajectories of d_1 and d_2 when applying the proposed control scheme under (a) $\Delta L_1 = +10$ µH, $\Delta L_2 = +10$ µH, (b) $\Delta L_1 = +10$ µH, $\Delta L_2 = -10$ µH, (c) $\Delta L_1 = -10$ µH, $\Delta L_2 = +10$ µH and (d) $\Delta L_1 = -10$ µH, $\Delta L_2 = -10$ µH.

good agreement with the results in Fig. 6. Fig. 7(b) shows the waveforms of I_{1dc} and I_{2dc} before applying the LPF. I_{1dc} and I_{2dc} increase from approximately 1.4 A to 2 A. These results indicate that the maximum output power point is successfully being tracked by the P&O algorithm. Fig. 8 shows the AC waveforms measured at steady-state. I_{ksw} and V_{ksw} $(k = 1, 2)$ represent the current and voltage of the MOSFET implemented on the switched capacitor board. The waveforms of I_1 and I_2 are orthogonal to I_t, indicating that the reactance of RX1 and RX2 are successfully compensated by the switched capacitors.

Fig. 9 shows the trajectories of d_1 and d_2 when the proposed control scheme is applied against four patterns of self-inductance variations *i.e.* $(\Delta L_1, \Delta L_2)$ = $(+10\,\mu H, +10\,\mu H)$, $(+10\,\mu H, -10\,\mu H)$, $(-10\,\mu H, +10\,\mu H)$, $(-10\,\mu H, -10\,\mu H)$. Since it is difficult to directly change the self-inductance of the coils, the values of C_{11} and C_{21} are modified such that

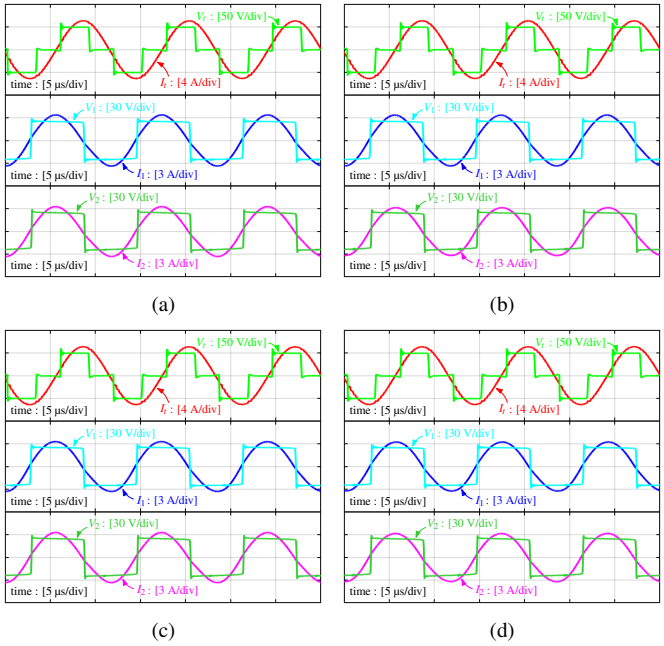

Fig. 10. AC waveforms measured at steady-state when the proposed control scheme is applied under (a) $\Delta L_1 = +10\,\mu\text{H}$, $\Delta L_2 = +10\,\mu\text{H}$, (b) $\Delta L_1 = +10\,\mu\text{H}$, $\Delta L_2 = -10\,\mu\text{H}$, (c) $\Delta L_1 = -10\,\mu\text{H}$, $\Delta L_2 = +10\,\mu\text{H}$ and (d) $\Delta L_1 = -10\,\mu\text{H}$, $\Delta L_2 = -10\,\mu\text{H}$.

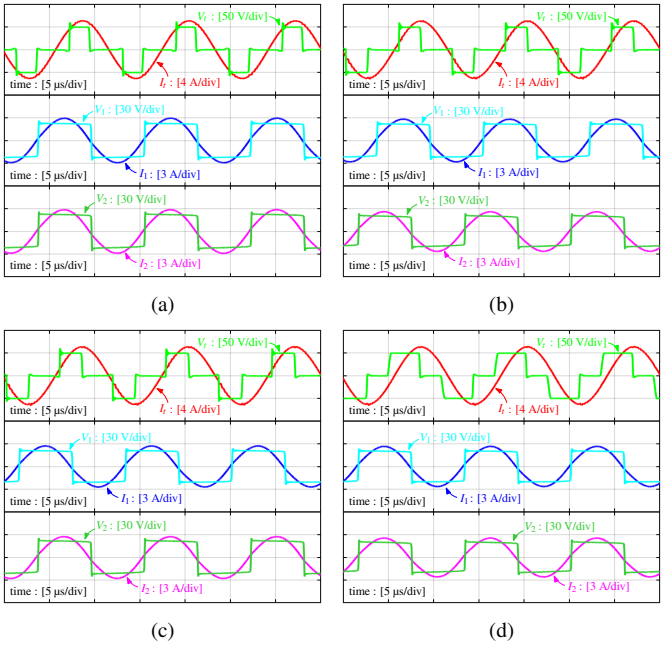

Fig. 11. AC waveforms measured at steady-state when passive capacitors are adopted to realize (a) $\Delta L_1 = +10\,\mu\text{H}$, $\Delta L_2 = +10\,\mu\text{H}$, (b) $\Delta L_1 = +10\,\mu\text{H}$, $\Delta L_2 = -10\,\mu\text{H}$, (c) $\Delta L_1 = -10\,\mu\text{H}$, $\Delta L_2 = +10\,\mu\text{H}$ and (d) $\Delta L_1 = -10\,\mu\text{H}$, $\Delta L_2 = -10\,\mu\text{H}$.

the impedance of the circuit is equal to the self-inductance variations. d_1 and d_2 converge to a lower value than 0.5 in Fig. 9(a) in order to compensate for the increase in the self-inductance of RX1 and RX2. On the other hand, d_2 converges to a higher value than 0.5 in Fig. 9(b) in order to compensate for the decrease in the self-inductance of RX2. The same argument can be applied to Figs. 9 (c) and (d). Fig. 10 shows the AC waveforms of the TX and RX circuits after the proposed control scheme converged to a steady state. It can be seen that the waveforms of I_1 and I_2 are orthogonal to I_t in both cases, indicating that the reactance of RX1 and RX2 are successfully compensated by the switched capacitors.

In order to evaluate the efficiency improvement provided by the proposed control scheme, the performance of the proposed control scheme is compared with cases in which passive capacitors are adopted instead of switched capacitors. The passive capacitors are chosen such that the impedance of the circuit is equal to $(\Delta L_1, \Delta L_2) = (+10\,\mu\text{H}, +10\,\mu\text{H})$, $(+10\,\mu\text{H}, -10\,\mu\text{H})$, $(-10\,\mu\text{H}, +10\,\mu\text{H})$, $(-10\,\mu\text{H}, -10\,\mu\text{H})$. Fig. 11 shows the AC waveforms of the TX and RX circuits when passive capacitors are adopted. In addition, Table II shows the comparison of the phase difference and efficiency measured at steady-state. As can be seen from Fig. 11 and Table II, the phase difference between I_t, I_1, and I_2 are far from optimal when passive capacitors are adopted. However, when the proposed control scheme is applied, $\angle I_1 - \angle I_t$ and $\angle I_2 - \angle I_t$ settle to approximately 90°, and the overall efficiency increases by up to 3.3%. The overall efficiency is increased since the transmission efficiency to each receiver is maximized by compensating for the self-inductance variations, as discussed in Section II-B.

TABLE II
COMPARISON OF PHASE DIFFERENCE AND EFFICIENCY.

		$\angle I_1 - \angle I_t$	$\angle I_2 - \angle I_t$	$\eta_1 + \eta_2$
$\Delta L_1 = +10\,\mu\text{H}$ $\Delta L_2 = +10\,\mu\text{H}$	w/ control	89.6°	89.3°	85.5%
	w/o control	63.2°	64.3°	82.5%
$\Delta L_1 = +10\,\mu\text{H}$ $\Delta L_2 = -10\,\mu\text{H}$	w/ control	89.9°	91.4°	85.3%
	w/o control	62.9°	128.1°	82.0%
$\Delta L_1 = -10\,\mu\text{H}$ $\Delta L_2 = +10\,\mu\text{H}$	w/ control	90.5°	89.7°	85.4%
	w/o control	127.3°	64.1°	82.1%
$\Delta L_1 = -10\,\mu\text{H}$ $\Delta L_2 = -10\,\mu\text{H}$	w/ control	91.1°	88.3°	85.4%
	w/o control	127.1°	127.9°	84.2%

These results verify the effectiveness of the proposed control scheme.

IV. CONCLUSION

This paper proposed a control scheme for PWM-controlled switched capacitors to compensate for the self-inductance variations in multiple-receiver WPT systems. The switched capacitors can adapt to the self-inductance variations of the RX coils by tracking the maximum output power point while regulating the amplitude of the TX current to a constant value. The proposed control scheme can be implemented by completely separate closed-loops on each circuit, thus eliminating wireless communication and additional circuits.

The effectiveness of the proposed control scheme was verified through experimental results.

The cross-coupling between the RX coils was not considered in this paper. When the RX coils are cross-coupled, the power flow to each receiver cannot be isolated by simply regulating the TX current, since the power is directly exchanged between the receivers [19], [20]. The improvement of the proposed control scheme considering this issue will be addressed in future work.

Another important topic which was not addressed in this paper is the output power control on each receiver. In practical applications, the output power of each receiver should be regulated to the desired value by active rectifiers or DC/DC converters. The integration of the control scheme proposed in this paper with the output power control will also be addressed in future work.

ACKNOWLEDGEMENT

This work was partly supported by JST-Mirai Program Grant Number JPMJMI21E2, JSPS KAKENHI Grant Number JP18H03768, and project JPNP21005 subsidized by the New Energy and Industrial Technology Development Organization (NEDO).

REFERENCES

[1] B. L. Cannon, J. F. Hoburg, D. D. Stancil, and S. C. Goldstein, "Magnetic resonant coupling as a potential means for wireless power transfer to multiple small receivers," *IEEE Transactions on Power Electronics*, vol. 24, no. 7, pp. 1819–1825, 2009.

[2] J. Kim, H.-C. Son, D.-H. Kim, and Y.-J. Park, "Impedance matching considering cross coupling for wireless power transfer to multiple receivers," in *2013 IEEE Wireless Power Transfer (WPT)*, 2013, pp. 226–229.

[3] Y. Zhang, T. Lu, Z. Zhao, F. He, K. Chen, and L. Yuan, "Selective wireless power transfer to multiple loads using receivers of different resonant frequencies," *IEEE Transactions on Power Electronics*, vol. 30, no. 11, pp. 6001–6005, 2015.

[4] Z. Pantic, K. Lee, and S. M. Lukic, "Receivers for multifrequency wireless power transfer: Design for minimum interference," *IEEE Journal of Emerging and Selected Topics in Power Electronics*, vol. 3, no. 1, pp. 234–241, 2015.

[5] Y.-J. Kim, D. Ha, W. J. Chappell, and P. P. Irazoqui, "Selective wireless power transfer for smart power distribution in a miniature-sized multiple-receiver system," *IEEE Transactions on Industrial Electronics*, vol. 63, no. 3, pp. 1853–1862, 2016.

[6] L. Sun, H. Tang, and S. Zhong, "Load-independent output voltage analysis of multiple-receiver wireless power transfer system," *IEEE Antennas and Wireless Propagation Letters*, vol. 15, pp. 1238–1241, 2016.

[7] S. Kisseleff, I. F. Akyildiz, and W. H. Gerstacker, "Magnetic induction-based simultaneous wireless information and power transfer for single information and multiple power receivers," *IEEE Transactions on Communications*, vol. 65, no. 3, pp. 1396–1410, 2017.

[8] M. Fu, H. Yin, M. Liu, Y. Wang, and C. Ma, "A 6.78 mhz multiple-receiver wireless power transfer system with constant output voltage and optimum efficiency," *IEEE Transactions on Power Electronics*, vol. 33, no. 6, pp. 5330–5340, 2018.

[9] X. Chen, S. Yu, and Z. Zhang, "A receiver-controlled coupler for multiple output wireless power transfer applications," *IEEE Transactions on Circuits and Systems I: Regular Papers*, vol. 66, no. 11, pp. 4542–4552, 2019.

[10] R. Narayanamoorthi, A. Vimala Juliet, and B. Chokkalingam, "Cross interference minimization and simultaneous wireless power transfer to multiple frequency loads using frequency bifurcation approach," *IEEE Transactions on Power Electronics*, vol. 34, no. 11, pp. 10 898–10 909, 2019.

[11] W. Cai, H. Tang, X. Lai, and L. Sun, "Multiple-receiver wireless power transfer with efficient power control strategy," in *2019 IEEE PELS Workshop on Emerging Technologies: Wireless Power Transfer (WoW)*, 2019, pp. 378–382.

[12] Y. Xiao, C. Liu, Y. Huang, and S. Liu, "Concurrent wireless power transfer to multiple receivers with additional resonant frequencies and reduced power switches," *IEEE Transactions on Industrial Electronics*, vol. 67, no. 11, pp. 9292–9301, 2020.

[13] G. Ning, P. Zhao, R. He, and M. Fu, "A novel passive current sharing method for a two-receiver-coil ipt system," in *2020 IEEE PELS Workshop on Emerging Technologies: Wireless Power Transfer (WoW)*, 2020, pp. 354–357.

[14] S. B. Lee, M. Kim, and I. G. Jang, "Determination of the optimal resonant condition for multireceiver wireless power transfer systems considering the transfer efficiency and different rated powers with altered coupling effects," *IEEE Journal of Emerging and Selected Topics in Power Electronics*, vol. 9, no. 2, pp. 2384–2393, 2021.

[15] Z. Zhang, H. Pang, S. H. K. Eder, and R. Kennel, "Self-balancing virtual impedance for multiple-pickup wireless power transfer," *IEEE Transactions on Power Electronics*, vol. 36, no. 1, pp. 958–967, 2021.

[16] T. Imura and Y. Hori, "Maximizing air gap and efficiency of magnetic resonant coupling for wireless power transfer using equivalent circuit and neumann formula," *IEEE Transactions on Industrial Electronics*, vol. 58, no. 10, pp. 4746–4752, 2011.

[17] D.-H. Kim and D. Ahn, "Self-tuning lcc inverter using pwm-controlled switched capacitor for inductive wireless power transfer," *IEEE Transactions on Industrial Electronics*, vol. 66, no. 5, pp. 3983–3992, 2019.

[18] S. Ann and B. K. Lee, "Analysis of impedance tuning control and synchronous switching technique for a semibridgeless active rectifier in inductive power transfer systems for electric vehicles," *IEEE Transactions on Power Electronics*, vol. 36, no. 8, pp. 8786–8798, 2021.

[19] M. Ishihara, K. Fujiki, K. Umetani, and E. Hiraki, "Autonomous system concept of multiple-receiver inductive coupling wireless power transfer for output power stabilization against cross-interference among receivers and resonance frequency tolerance," *IEEE Transactions on Industry Applications*, vol. 57, no. 4, pp. 3898–3910, 2021.

[20] X. Xie, C. Xie, Y. Li, J. Wang, Y. Du, and L. Li, "Adaptive decoupling between receivers of multireceiver wireless power transfer system using variable switched capacitor," *IEEE Transactions on Transportation Electrification*, vol. 7, no. 4, pp. 2143–2155, 2021.

[21] S. Li, W. Li, J. Deng, T. D. Nguyen, and C. C. Mi, "A double-sided lcc compensation network and its tuning method for wireless power transfer," *IEEE Transactions on Vehicular Technology*, vol. 64, no. 6, pp. 2261–2273, 2015.

[22] R. Matsumoto and H. Fujimoto, "Wireless ev charging system using pwm-controlled variable capacitor for maximum power transfer under severe coil misalignment," in *2022 International Power Electronics Conference (IPEC-Himeji 2022- ECCE Asia)*, 2022, pp. 1476–1480.

[23] F. Grazian, T. B. Soeiro, and P. Bauer, "Inductive power transfer based on variable compensation capacitance to achieve an ev charging profile with constant optimum load," *IEEE Journal of Emerging and Selected Topics in Power Electronics*, pp. 1–1, 2022.

[24] R. Matsumoto and H. Fujimoto, "Adaptive compensation scheme for wireless power transfer systems with coil inductance variation using pwm-controlled switched capacitor," in *2022 Wireless Power Week (WPW)*, 2022, pp. 244–248.

[25] Z. Ma, M. Xiao, Y. Xiao, Z. Pang, H. V. Poor, and B. Vucetic, "High-reliability and low-latency wireless communication for internet of things: Challenges, fundamentals, and enabling technologies," *IEEE Internet of Things Journal*, vol. 6, no. 5, pp. 7946–7970, 2019.

[26] N. Femia, G. Petrone, G. Spagnuolo, and M. Vitelli, "Optimization of perturb and observe maximum power point tracking method," *IEEE Transactions on Power Electronics*, vol. 20, no. 4, pp. 963–973, 2005.